Springer Link

Microfluidics and Nanofluidics
© Springer-Verlag Berlin Heidelberg 2013
10.1007/s10404-013-1225-6

Research Paper

High-speed counting and sizing of cells in an impedance flow microcytometer with compact electronic instrumentation

Oscar Castillo-Fernandez[1,2,3], Romen Rodriguez-Trujillo[4], Gabriel Gomila[3,5] and Josep Samitier[1,2,3]

(1) Nanobioengineering Group, Institute for Bioengineering of Catalonia (IBEC), Baldiri Reixac 10-12, 08028 Barcelona, Spain

(2) Centro de Investigación Biomédica en Red en Bioingeniería, Biomateriales y Nanomedicina (CIBER-BBN), C/María de Luna 11, Edificio CEEI, 50018 Zaragoza, Spain

(3) Department of Electronics, University of Barcelona, Martí i Franquès 1, 08028 Barcelona, Spain

(4) Department of Micro- and Nanotechnology, DTU Nanotech, Technical University of Denmark, Building 345E, Kgs. Lyngby, Denmark

(5) Nanobioelectricity Group, Institute for Bioengineering of Catalonia (IBEC), Baldiri Reixac 10-12, 08028 Barcelona, Spain

Oscar Castillo-Fernandez
Email: oscartillo@gmail.com

Received: 24 February 2013
Accepted: 20 June 2013
Published online: 9 July 2013

Abstract

Here we describe a high-throughput impedance flow cytometer on a chip. This device was built using compact and inexpensive electronic instrumentation. The system was used to count and size a mixed cell sample containing red blood cells and white blood cells. It demonstrated a counting capacity of up to ~500 counts/s and was validated through a synchronised high-speed optical detection system. In addition, the device showed excellent discrimination performance under high-throughput conditions.

Keywords Microcytometry – Microfluidics – Impedance – Electronics – Red blood cells (RBCs) – White blood cells (WBCs)

1 Introduction

The development of integrated cell counters and analysers is of vital importance in medicine and biology. In order to understand fundamental processes of the cell and also to detect and monitor a number of diseases (AIDS, cancer, malaria, etc.), devices or technology with the capacity to detect changes in cell volume, surface morphology, structure or composition is required. Flow cytometers are widely used in hospitals and laboratories to perform these types of studies (Shapiro *1995*). However, conventional flow cytometers are very expensive instruments and have limited portability and integration with other cell analysis equipments. Therefore, a compact, portable and low-cost alternative would be desirable to be used as a stand-alone version or integrated in a lab-on-a-chip device.

The literature provides several examples of flow cytometers adopting microfabrication technology and using several detection approaches (electric, light sensor, etc.) (Huh et al. *2005*; Zhang et al. *2009*). Electric detection is one of the most common approaches because of its straightforward integration and miniaturisation. In this field, the use of electrical impedance detection methods to extract a variety of useful information from cells has been widely reported. A recent review (Sun and Morgan *2010*) informed that many groups are working in microcoulter counters utilising impedance detection strategies. These electronic microcytometers have acquired a higher profile because of a significant increase in their performance, for instance by using multiple frequencies for cell identification purposes. Impedimetric microcoulter counters use AC currents to detect impedance variations caused by cell transitions over pairs of microelectrodes aligned perpendicular to microfluidic channels (Ayliffe et al. *1999*; Sohn et al. *2000*; Gawad et al. *2001*).

A number of strategies are used to transduce the impedance variations in a suitable electric signal. Gawad et al. (*2001*) presented a sensing strategy based on a Wheatstone bridge in order to transduce impedance changes to a voltage signal. That study used a lock-in amplifier to demodulate the transduced signal. This system was later used to count and differentiate red blood cells (RBCs) from polystyrene beads, ghosts and fixed RBCs (Cheung et al. *2005*). Also, Nieuwenhuis used a trans-impedance amplifier as a transducer and a commercial lock-in amplifier for detection (Nieuwenhuis et al. *2004*).

In the case of highly integrated systems or low-cost systems, simpler detection schemes may be advisable. As an alternative, in a previous study, we presented a compact and low-cost instrument that does not require lock-in detection schemes for cell counting in impedance flow cytometers (Rodriguez-Trujillo et al. *2008*). The electronics allowed the high-speed counting of latex particles and yeast cells. However, the capacity of this simple instrumentation scheme for high-throughput sizing particles has not been demonstrated to date.

Here we go beyond these previous results and demonstrate the capacity of this simple electronic scheme to address particle sizing in complex samples such as blood cells. The sizing performance of

the system was validated directly by comparison with optical images obtained with a high-speed optical camera synchronised and coupled to the system. The high sensitivity and speed of the optical system implied no need for cell labelling, which is an advantage in front of previous optical validation approaches that used optical fluorescence detection schemes (Morgan et al. *2006*; Benazzi et al. *2007*; Holmes et al. *2007*, *2009*). In particular, the optical validation systems used here allowed us to track RBCs over time and compare their position and shape with the evolution of the resulting electronic signal. This possibility increased the available information and the capacity to calibrate the electronics and to adjust the detection algorithm for the detection of clusters and sizing, crucial parameters when dealing with biological samples.

2 Materials

Figure 1 shows the validated system, which comprises a microfluidic impedance flow cytometer device and the electronic board used for signal generation and processing. The microfluidic device is a glass-polymer device with integrated gold microelectrodes that will be described in detail in Sect. 2.1. The electronic system consists of two main boards: the signal demodulation board, which is presented and discussed in Sect. 2.2, and the power and control board. The latter implements several elements, such as power control of the whole system and a function generator to supply the AC excitation signal for detection.

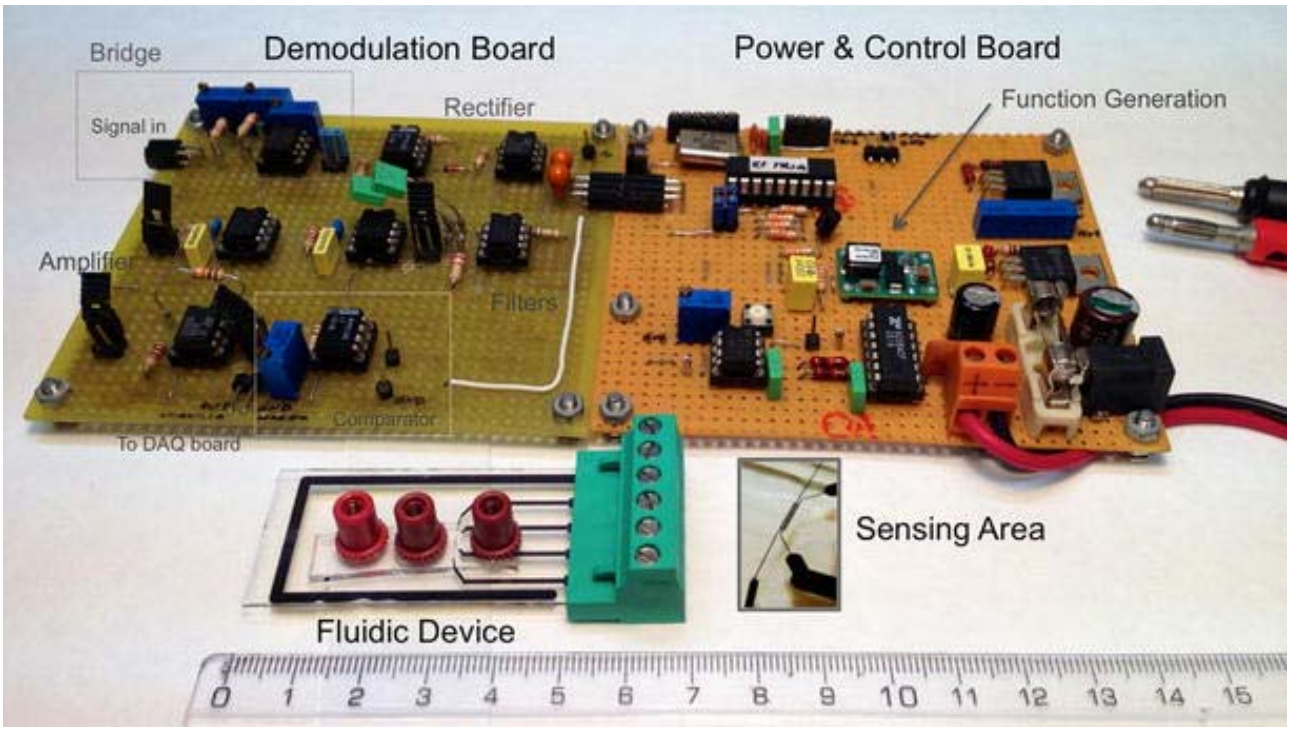

Fig. 1

Picture of the impedance counter system composed of the electronic system and the microfluidic device. The latter is a glass-polymer device with integrated gold microelectrodes. The *green board* comprises the counting circuit. The *orange board* contains several elements, such as the power control

of the whole system and the function generator (colour figure online)

2.1 Fabrication of the microfluidic device and sample preparation

The microfluidic chip consists of a single microchannel with coplanar perpendicular electrodes, where the cell alignment is achieved by physical constriction. Two different chips were fabricated with channel cross sections of 10 μm × 10 μm and 20 μm × 20 μm, with a channel length constriction of 1 mm. The detection electrodes were 20 μm wide separated by 10 μm. Four electrodes were fabricated, a[illegible]nts. Two inlets were implemented in the device to [illegible]iguez-Trujillo et al. *2008*), in order to force cells [illegible]s, thus reducing the lack of sensitivity related to the c[illegible]

Would you use a data collaboration website to share your research data with colleagues?

Yes, publicly

Yes, but only privately

No

I don't have data

The channel was fabricated [illegible]made by means of standard SU8 photolithograp[illegible]ealed with a glass cover by oxygen plasma bonding. [illegible]r by means of a lift-off technique using a reversible p[illegible]al deposition of 20 nm of Ti and 80 nm of Au by evaporation.

RBCs were obtained from whole blood using standard centrifugation. Samples were centrifuged three times to reduce contamination from plasma or other elements such as platelets. Afterwards, the RBCs were diluted to an approximate concentration of 10^7 cells/ml with phosphate-buffered saline (PBS) with a measured conductivity of 1.6 S/m. PBS is a commonly used buffer for living cells because it is isotonic and has a similar conductivity to that of blood plasma.

White blood cells (WBCs) were obtained from the THP-1 monocyte cell line culture. These cells were centrifuged and diluted with PBS to a concentration of approximately 10^5 cells/ml. The mixed cell buffer was obtained by mixing RBCs and WBCs buffers at a ratio of 1:1.

2.2 The detection circuitry

We used a Wheatstone bridge to convert the changes in impedance to a read-out voltage. Two pairs of electrodes were located at different branches of the bridge, as shown in Fig. 2a. The transduction system included an instrumentation amplifier with a gain of 100 times and two resistors, Rp1 and Rp2, to form the additional branches of the bridge.

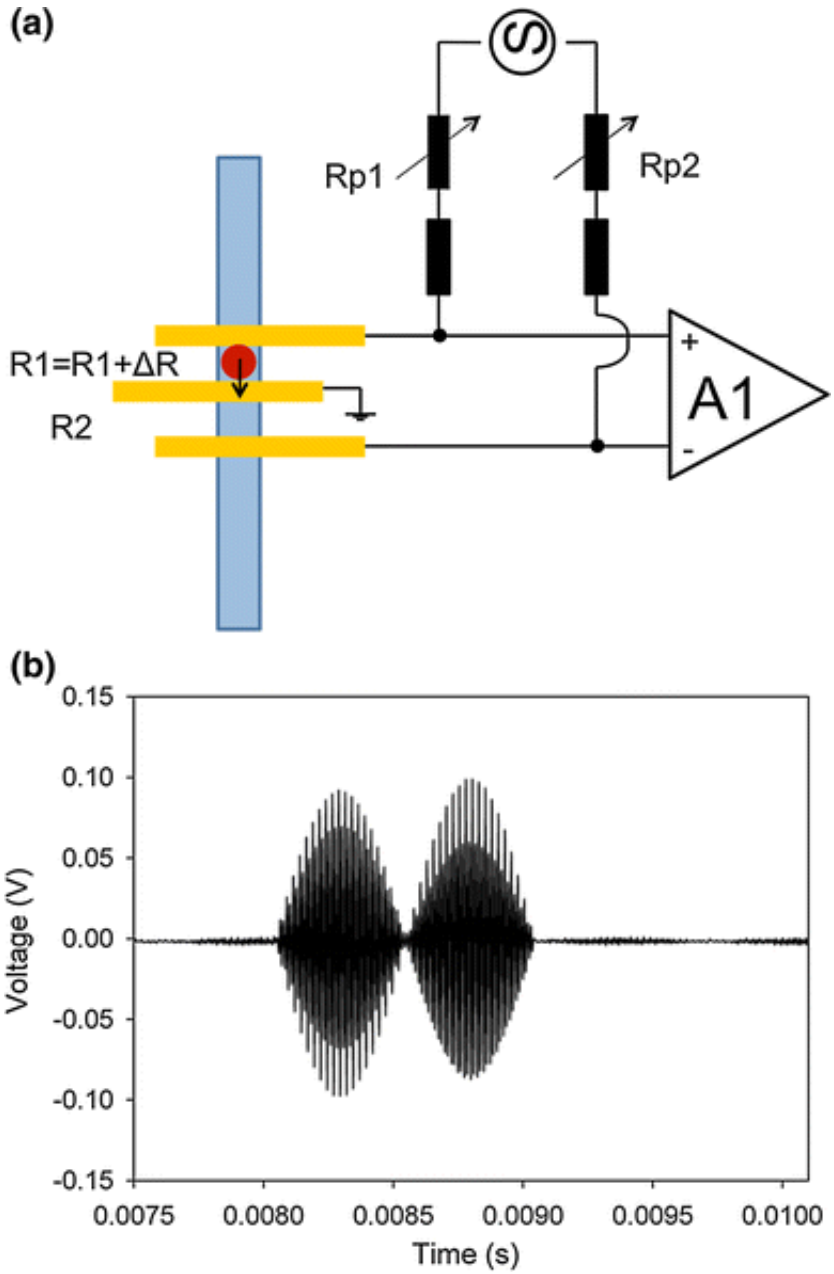

Fig. 2

a Layout of the Wheatstone bridge with connections to the measuring electrodes. A potentiometer was used to equilibrate the bridge. *A1* is an instrumentation amplifier with a 100 times gain. **b** Theoretical electric signal corresponding to the transition of a particle over the electrodes connected to the Wheatstone bridge

The frequency range of operation was chosen to coincide with the range in which capacitive effects are smaller and low enough to detect a cell as an electrically opaque object (Gawad et al. *2004*). The resistor values were chosen according to the measured impedance between a pair of electrodes (50–100 kΩ), measured with an impedance analyser (Agilent 4294A) in the frequency range of operation (10^5–10^6 Hz). Thus, the resistors Rp1 and Rp2 were designed with a potentiometer (0–20 kΩ) and a standard resistor (40 kΩ), in order to have an impedance range sufficient to allow satisfactory equilibrium conditions between the two branches of the bridge. To avoid effects on the fluid that could damage samples and electrodes, the amplitudes used to stimulate the bridge were lower than 1 V.

Under ideal conditions in which the bridge can be completely balanced, the output of the differential amplifier A1 in Fig. 2a should give 0 V. Therefore, when a particle crosses the first pair of electrodes, the voltage between the two electrodes is increased as a result of the higher impedance, and the amplifier output will follow the increasing voltage, leading to an increase in the signal amplitude. Moreover, when the particle crosses the second pair of electrodes, the same effect will occur with 180º phase, because of the negative input of the amplifier. Taking into account that the stimulus of the bridge is an AC signal, the effect of a cell crossing the sensing zone is an amplitude modulation of a known oscillating signal. An example of the type of modulation expected by the passage of a cell is shown in Fig. 2b, for the case of a particle with a comparable size to the electrode dimensions and their separation. This signal was created using a base sinus of 120 kHz, which was modulated in amplitude by a square signal of 2 kHz frequency and 1 ms duration, representing the cell transition.

The detected phase of the impedance between a pair of electrodes in the frequency range of operation was around −50°, meaning that the response of the system was not fully resistive. The presence of capacitive effects in the response of the electrodes was caused by their small area and separation, which is unavoidable for high-throughput detection with microelectrodes. These effects hindered the complete equilibration of the bridge since only resistive elements were used to equilibrate the impedance differences between the two pairs of electrodes. However, as shown later on, this drawback did not limit the performance of the device.

The relevant information describing the particle transition dynamics corresponds to the envelope of the electric signal. The circuit chosen here for signal processing was therefore a standard architecture for amplitude demodulation: one rectifier step followed by the extraction of the envelope by a low-pass filter step. A further high-pass filter to remove any signal offset and a final amplification were also added to the basic set-up, as shown in Fig. 3 (upper row). The filters used were Sallen-key architectures. The low-pass filter was a fourth-order filter with 10 kHz cut-off frequency with a quality factor of 0.5, while the high-pass filter was a second-order filter with 7 Hz cut-off frequency with a quality factor of 0.5.

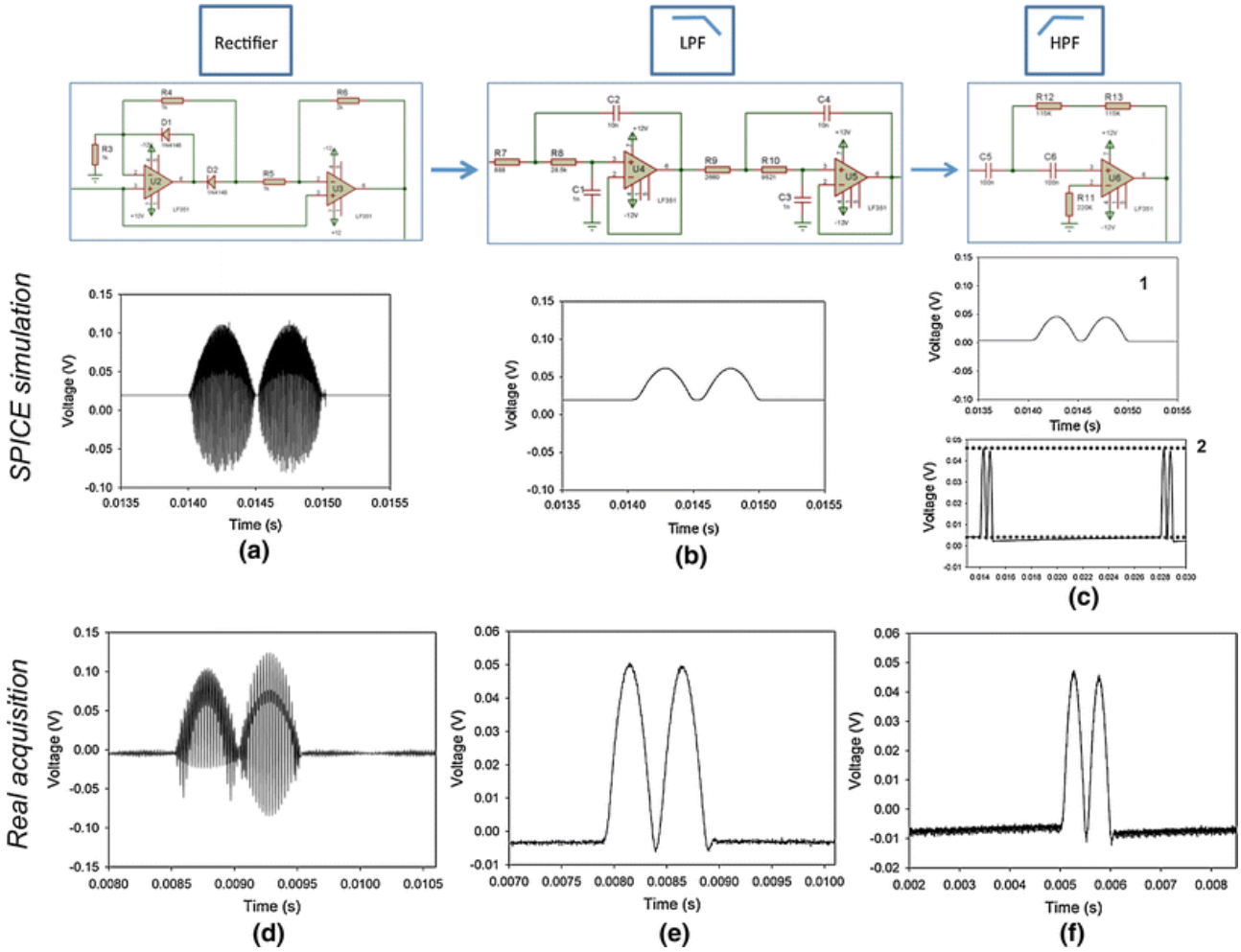

Fig. 3

Representation of each modular part of the demodulator system and the response of the SPICE model when the signal plotted in Fig. 2b was applied. The rectifier (**a**) follows a fast and low-amplitude signal, and the low-pass filter (**b**) gives the envelope of the signal. The signal is further centred on zero by the high-pass filter (**c**), resulting in low deformation of the signal (**c**-2). The true response of the electronic device was obtained for each module by applying the model signal (Fig. 2b) using a programmable signal generator. Note that the signals obtained are identical to those modelled on SPICE, including the small deformation generated by the high-pass filter (**f**)

This architecture was initially implemented using SPICE simulation software to validate the electronic design. In Fig. 3b the effect of the rectifier and the low-pass filter, which gives the envelope of the signal, and the effect of the high-pass filter are shown. When a noisy signal is present due to non-optimal balance between the two branches of the bridge or even ambient noise, the relative amplitude signal generated by a particle is reduced. In order to minimise this effect, a high-pass filter was used to subtract the offset. The low-pass filter decreases the power of the signal, reducing the amplitude because of the removal of some of the frequency components. The high-pass filter has an effect on the shape of the signal, i.e. it reduces the mean value of the signal, which deforms the second peak, as shown by the dotted line in Fig. 3(c-2). A secondary effect is that a stabilisation time appears after each transition.

A digital signal was generated by a LabVIEW program and loaded as an arbitrary form using a function generator (TABOR Electronics. WW5061). The resulting signal was applied to the

electronic system. The results of each step, namely rectification, low-pass filter and high-pass filter, were acquired with a National Instruments acquisition board, controlled with a LabVIEW program, and are displayed in Fig. 3(d–f). The device displayed a response that was in complete agreement with the SPICE model simulated previously.

2.3 Optical detection system

In order to validate that the transitions acquired with the electronic instrumentation were due to the cell crossing the sensing zone, we synchronised a fast microscope camera (Photron FastCam 1024) mounted on an inverted microscope (Olympus IX71) with the impedance detection system so that we could simultaneously record high-speed images of the RBCs travelling across the electrode array and the corresponding electric signal. An external trigger was used to define a common starting time point, from where it was possible to identify the images corresponding to each electrical transition by knowing the frame rate of each acquisition system.

---

3 Results and discussion

3.1 Cell detection: electronic validation

Once the circuit had been modelled, fabricated and tested, the demodulation system was used to detect and quantify biological cell populations flowing through the microfluidic device. The system was validated with experiments carried out using RBCs. The validation involved verifying the capacity of the instrumentation to detect cell transitions over the electrodes.

Figure 4 shows several signals corresponding to particle transition recorded with two configurations of the Wheatstone bridge. In both cases, the sample flow rate was kept constant at 0.1 μL/min, resulting in a theoretical mean velocity at the sensing area of 31.9 μm/ms (Berthier and Silberzan *2005*), thus implying a transition duration of 3 ms. In order to gain a better understanding of the detection of the cell transition, we acquired the signal at the end of the Wheatstone bridge (first column in Fig. 4) and after the demodulation (second column in Fig. 4). The results were also compared to the mathematical result obtained from a MATLAB program, which simulated the effect of the electronic filters on the signals recorded after the Wheatstone bridge (last column in Fig. 4). The result of the MATLAB operation is shown by the green traces.

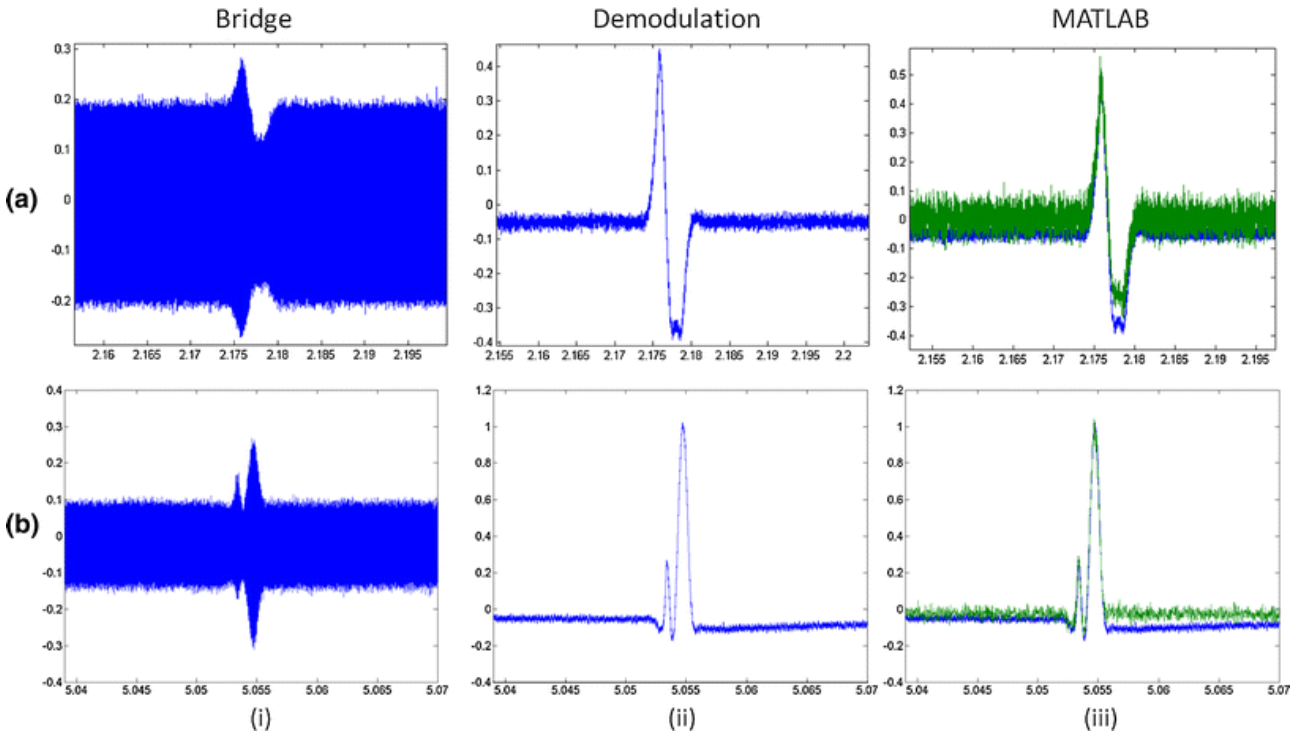

Fig. 4

Study of the shape of recorded signals when the equilibrium of the bridge was changed. Two bridge configurations are considered in **a** and **b**. The signals plotted in *blue* are the main signals recorded from the electronic circuit when a RBC crosses the sensing area; the bridge signals (*i*) are recorded from the output of the amplifier of the bridge, A1, in Fig. 2a. The demodulation signals (*ii*) are recorded after completion of the demodulation process. The MATLAB plots (*iii*) are the comparison between the demodulation signal from the electronic system (*blue*) and the signal obtained with a MATLAB simulation of the filters using the bridge signal (*green*). **a** shows a cell transition when the bridge was equilibrated to obtain a base-out signal of 400 mV peak to peak, while in **b** the bridge was fixed and equilibrated to 240 mV peak to peak (colour figure online)

Two characteristic signals were obtained under normal operation conditions, shown in Fig. 4a and b. The signal in Fig. 4a, compared to the ideal one, has only one increasing modulation effect because the cell transition on the second pair of electrodes appears as a reduction in amplitude, instead of a peak. These types of signals are obtained when the variation in impedance due to the particle is lower than the base impedance difference between branches, because the bridge is not fully balanced. This observation is confirmed in Fig. 4b by a transition signal displaying a double peak (similar to the one in Fig. 3). This signal was obtained by fine-tuning the bridge, resulting in the high equilibration of the bridge and a low-noise output signal, around 240 mV peak to peak.

It is important to emphasise here that although the true signals did not show the ideal profiles shown in Fig. 3 because of the non-purely resistive response of the system at the stimulation frequency, this did not impair counting or sizing performance of the device.

3.2 Cell detection: optical validation

Figure 5 shows six images of a cell crossing the sensing zone in specific positions on the electrode array, acquired with the high-speed optical system. The measurement was taken for a bridge

equilibrium set-up, resulting in a 200 mV peak to peak signal. The flux velocity was fixed at 0.5 µL/min with a time transition of 1 ms. The sensing electrodes, which formed the bridge, are the first three electrodes from the left. The time of each image is indicated in the images. Below the images, the signal recorded from the bridge is plotted in blue and the final demodulation in green. The red numbered bars indicate the synchronised times of acquisition with the numbered images. A clear correlation is observed between the electric signal and the optical images, unambiguously proving that the electric signal reflects the transition of a single RBC. In particular, when the RBC crossed the first pair of electrodes, it increased the amplitude of the difference between the two branches of the bridge, with a maximum when the particle was in the middle of one pair of electrodes, as for example between one and ground (see Fig. 5 image 3). Moreover, when the cell crossed the next two pairs of electrodes, the impedance effect was a subtraction because it was the negative input of the amplifier (see Fig. 5 image 4). The demodulation of the electric signal (blue line) gives the recorded electric signal (green line) with the shape already discussed above.

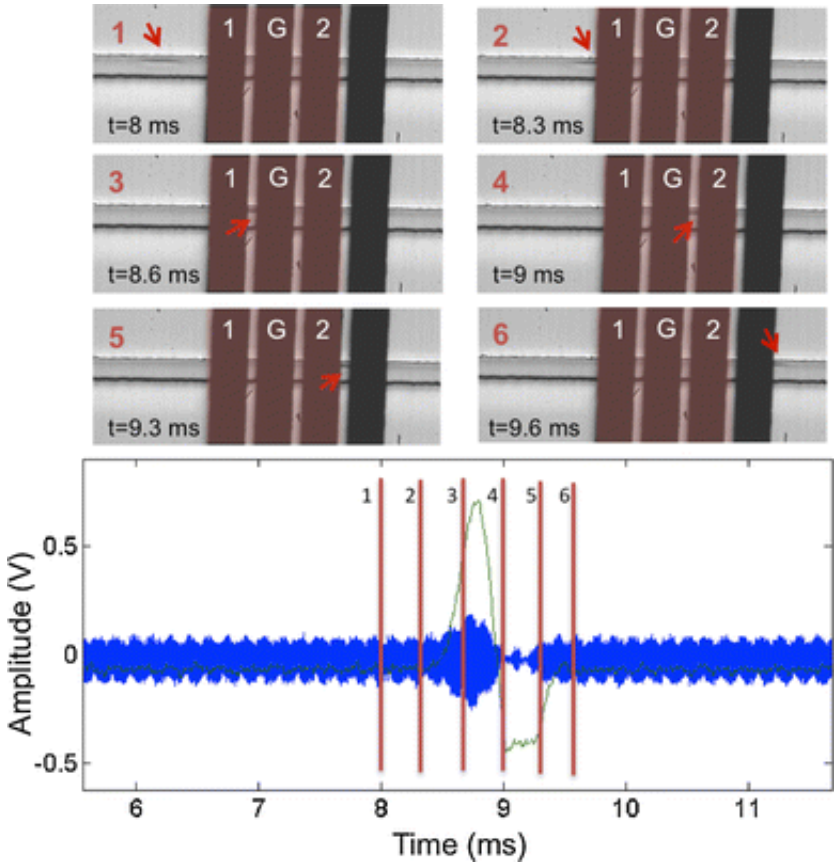

Fig. 5

Representation of the synchronisation of an optical acquisition of a cell crossing the sensing electrodes and the signals recorded from the electronic circuit (*blue one* from the bridge and *green one* from the final output of the demodulation process). The images were taken at various stages: outside of the sensing zone (*1*,*6*); close to the electrode array (*2*,*5*); and inside the electrode array: first pair of electrodes (*3*) and second pair (*4*). The *red bars* on the signal plot represent the time points at which images were recorded (colour figure online)

We used this optical system to validate more than 200 transitions, and the reliability of the electrical recording system was proved to be above 95 %. The remaining 5 % of transitions were detected by

the electronic system but not with the optical one. These errors were attributed to the focal distance at which images were taken and the movement of the cell in a different plane and thus invisible to the microscope camera. This notion is supported by the lower electric amplitude of the corresponding transitions detected, meaning that the cells were travelling far away from the electrodes where the microscope was focused. Additional experiments performed at lower velocities confirmed that a small proportion of the cells travelled out of focus and could not be recorded optically under the high-speed imaging conditions used. Therefore, we conclude that the reliability of the electronic detection system is greater than 95 %, approaching 100 %.

3.3 Cell detection capacity

3.3.1 Counting rate

First, the system was tested to demonstrate the capacity to detect particles under high-throughput conditions. In order to demonstrate the counting rate capacity of the impedance cytometer, we used a dilution of RBCs with an approximate concentration of 10^7 cells/ml. The channel constriction used had a cross section of 10 μm × 10 μm.

Figure 6 shows a scatter plot in which we show the amplitude of the electrical signal recorded as a function of the transition time. The amplitude is defined as the maximum potential reached by the signal, while the transition time is defined as the time between the two produced peaks when the particle is in the middle of the electrode pairs. This figure shows the transitions obtained from five consecutive acquisitions of 8.8 s (44 s) under a sample flow rate of 1 μL/min while the vertical focusing was fixed at 2 μL/min. These vertical focusing conditions limited the section occupied by the sample to a width of 10 μm wide and a height of 3.3 μm. In the electric signals, amplitudes above 0.01 V (corresponding to the noise of the system) were taken to correspond to particle transitions. A total of 20,422 cells were detected. This figure implies a true sampling rate of 464 cells/s. The resulting density of cells calculated on the basis of the sample flow rate used in this acquisition was $2.78 \cdot 10^7$ cells/ml, which is in agreement with the density prepared. In addition, the mean transition time was 0.13 ms, indicating a potential sample rate of a few thousands particles/s, which would be achievable for a higher concentration of samples. The amplitude of the transitions shows a mean value of 0.1 V with a standard deviation of 0.02 V. The low dispersion of these transitions shows that most of the cells passed at similar distances from the electrodes.

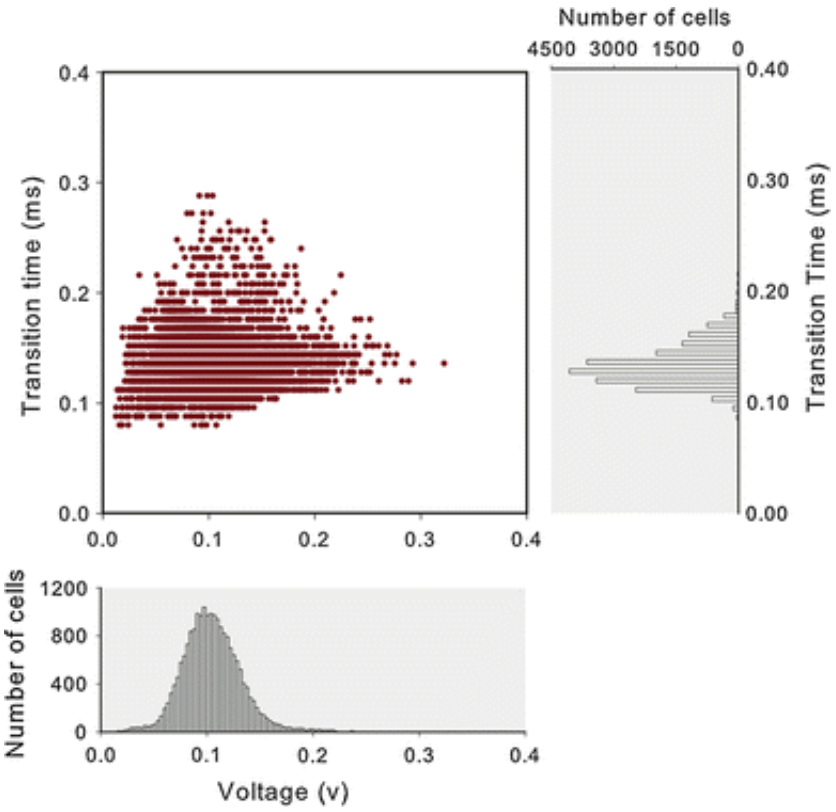

Fig. 6

Scatter plot relating the electrical amplitude obtained with the transition time for each transition. The histograms represent in detail the distribution of the two variables. In this scatter plot we show 20,422 electric transitions obtained in 44 s from a sample with approximately 10^7 cells/ml. The threshold used for particle detection was 0.01 V

3.3.2 Sizing

In order to demonstrate the size discrimination capacity of the impedance cytometer, we performed experiments using a mixed dilution of RBCs and WBCs (monocytes from the THP-1 cell line). The cell mixture was made with a concentration of approximately 10^7 cells/ml of RBC and 10^5 cells/ml of WBC.

The channel constriction used in this case had a cross section of 20 μm × 20 μm. Given that at the frequency of 120 kHz the impedance increment of the electrode pairs was due to the electrical opacity of the cell, the resulting transition amplitudes were expected to depend on cell volume.

Figure 7a shows the scatter plot corresponding to three consecutive acquisitions of 8.8 s (26.4 s) under hydrodynamic conditions of a sample flow rate 1 μL/min, while the vertical focussing flow rate was set at 0.1 μL/min (no focussing condition). Figure 7b shows a normalised histogram of the transition distribution by voltage amplitude. The histogram is normalised by the number of cells obtained below and over the threshold of 0.1 V independently. This histogram shows two distinct cell distributions. Using this threshold, we verified that of the 5,114 cells counted from the sample mixture, 28 showed a signal amplitude over 0.1 V. The cell concentrations obtained were $1.16 \cdot 10^7$ RBCs/ml and $0.63 \cdot 10^5$ WBCs/ml.

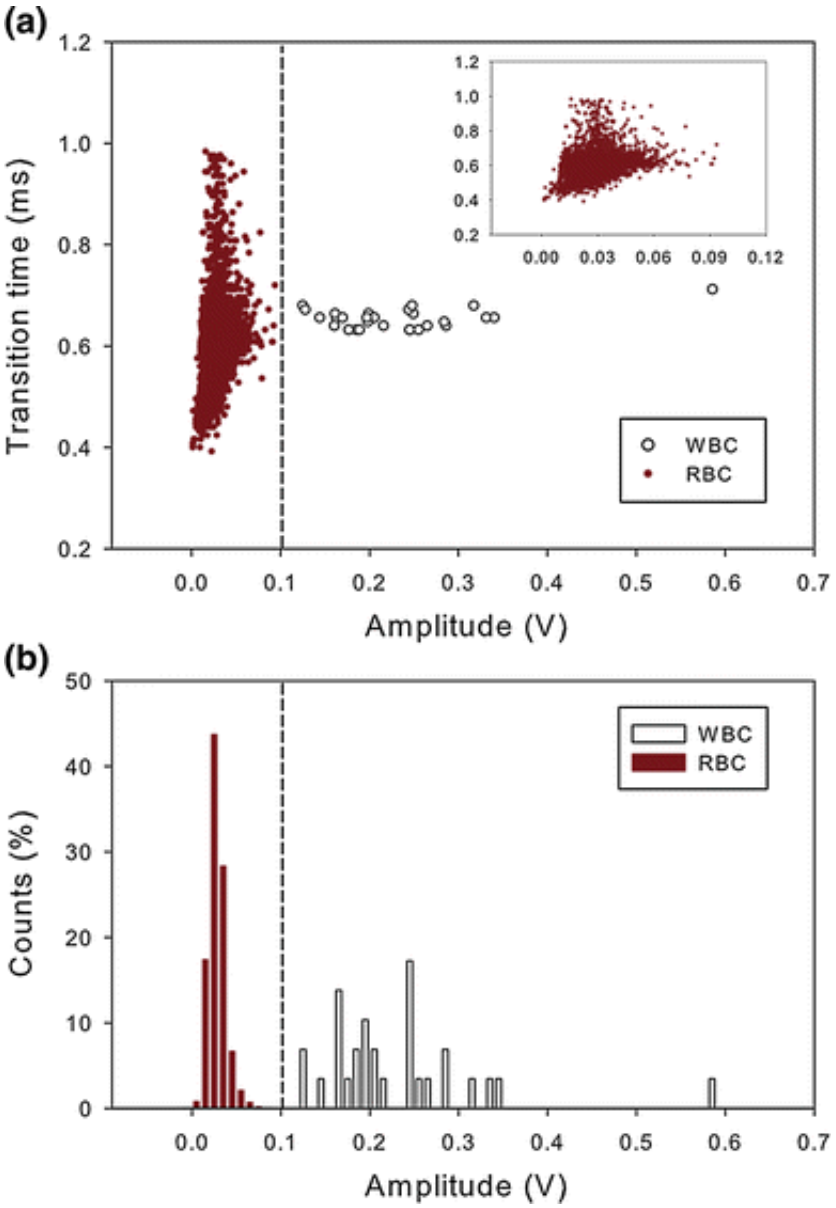

Fig. 7

Scatter plot (**a**) and the corresponding amplitude histogram (**b**) of transitions detected, of three consecutive acquisitions of 8.8 s (26.4 s) under the same hydrodynamic conditions. The absolute cell detection threshold was fixed at 0.01 V (system noise), and the threshold separating RBCs from WBCs was determined to be 0.1 V (further optically confirmed). The histogram represents the normalised number of counts relative to the total number of cells detected by the threshold method. The *inset* in (**a**) represents the population below 0.1 V at different axis scale, showing the same distribution of RBCs as in Fig. 6

Using the optical validation system, we proved that the low-amplitude peak distribution in the histogram corresponds to RBCs, while the higher-amplitude peak corresponds to WBCs. To this end, a number of cell transitions were recorded electrically and optically for a fixed bridge equilibrium and hydrodynamic conditions identical to those used in the experiment shown in Fig. 7. We then specifically selected a few in which the distance of the cells relative to the electrodes was similar. The volume of the cells was calculated from their diameter, estimated from the camera image using the image-processing software (Image J). These calculations have an associated systematic error because of the definition of the contour cell on the image, where a pixel denotes 0.44 μm. The error associated with the volume evaluation is obtained by a propagation error of ±1 μm on the

diameter measurement. Taking into account cell morphology, RBCs were modelled as discs with a thickness taken from the literature (2.5 μm). In contrast, WBCs were considered as spheres with a diameter measured from the images. Figure 8 shows the amplitude of the electrical signals as a function of the volume measured from the optical images. We obtained an almost linear relation between the amplitude of the electric transition and the volume calculated for each cell, thus indicating the suitability of the device for sizing applications. Moreover, the RBC population, clearly identifiable in the optical images, showed amplitudes below 0.1 V, in agreement with the threshold obtained from the histogram analysis shown above. Furthermore, the 10 selected WBC transitions had a mean value of 0.25 V, which correlated with the mean value of the population shown in Fig. 7. Figure 8 presents lower deviations for the two cell types than the population shown in Fig. 7, due to the restriction on the cell position from electrodes in Fig. 8. It is important to note the presence of some (n = 2) anomalous large THP-1 cells, which showed a significant difference in amplitude and volume, which the system detected and differentiated from the normal population.

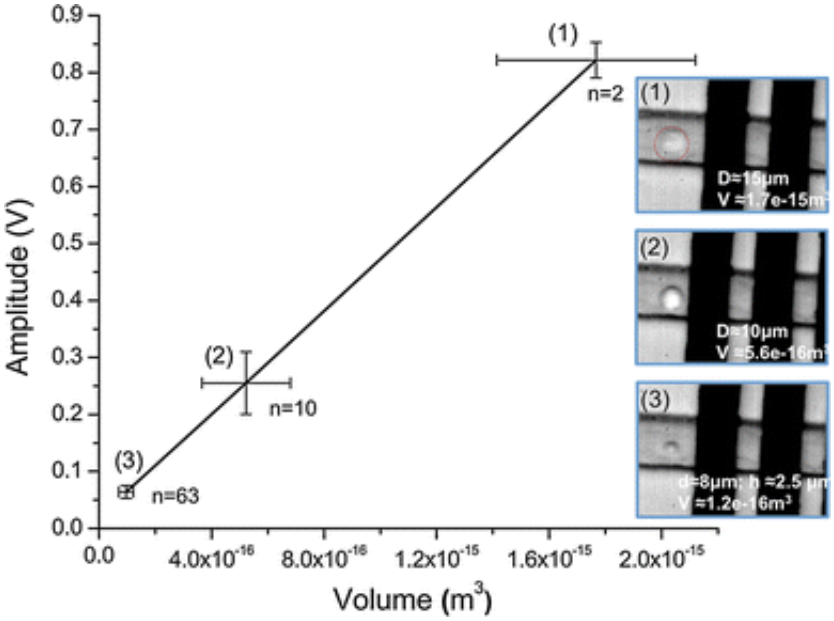

Fig. 8

Relationship between the cell volume and the electric amplitude of the recorded signals obtained in the device with a 20 μm × 20 μm cross-sectional channel. Under the same bridge conditions, the amplitude of the transition has a linear dependence with the cell volume. The *insets* show an example of three distinct populations transiting close to the electrodes. For WBCs (*1* and *2*), the volume was calculated as spheres with a diameter measured by image-processing software. The volume of RBCs (*3*) was calculated as a cylinder with a diameter as measured and assuming a thickness of 2.5 μm. The *error bars* in amplitude of the electronic output refer to the standard deviation of the selected population, while the *error bar* in cell volume represents the estimated systematic error derived from the volume calculation

4 Conclusions

Here we developed a high-throughput impedance cell analyser based on a compact and inexpensive

electronic device and tested its capacity to count and size cells in a microfluidic system. The system was validated by means of a real-image high-speed optical system, allowing the monitoring of cells travelling at high speed across the sensing zone and hence enabling comparison of the electric signals and the optical images under high-throughput conditions.

The system demonstrated a mean counting rate of more than 400 cells/s and a capacity to detect very fast particle transitions with time intervals below 0.1 ms. Moreover, the system showed excellent sensitivity to cell size, allowing discrimination between RBCs and WBCs under high-throughput conditions and a variety of cell proportions (<1 %). Finally, a linear relationship between electric signal amplitude and cell volume was observed in a wide range of cell sizes.

In conclusion, this impedance cell analyser showed a performance comparable to other technologies based on more sophisticated and less compact electronics. Given its capacity, we propose this system as an excellent alternative for lab-on-a-chip systems requiring high integration and portability.

Acknowledgments

This study was funded by the ISCIII through the FIS project PI071162 and the Science Support Program of the *Fundación Botín*. R.R-T acknowledges funding from EU FP6 Marie Curie program CELLCHECK (035854-1). We kindly acknowledge Drs. Alfred Cortés and Francesc Miro from the Gene Translation laboratory of the *Institute for Research in Biomedicine* (IRB Barcelona) for their help and for providing the cell populations used in these experiments. The authors also thank Mohammad Ajine for MATLAB software development and Miquel Garrido for implementation of the electronic system. The lab-on-a-chip was fabricated in the Nanotechnology Platform of the *Institute for Bioengeneering of Catalonia* (IBEC).

References

Ayliffe HE, Frazier AB, Rabbitt RD (1999) Electric impedance spectroscopy using microchannels with integrated metal electrodes. J Microelectromech Syst 8(1):50–57
CrossRef

Benazzi G, Holmes D, Sun T, Mowlem MC, Morgan H (2007) Discrimination and analysis of phytoplankton using a microfluidic cytometer. IET Nanobiotechnol 1(6):94–101
CrossRef

Berthier J, Silberzan P (2005) Microfluidics for Biotechnology, vol 1. Artech House Publishers, Boston, Microfluidics for Biotechnology

Cheung K, Gawad S, Renaud P (2005) Impedance spectroscopy flow cytometry: on-chip label-

free cell differentiation. Cytometry A 65A(2):124–132
CrossRef

Gawad S, Schild L, Renaud P (2001) Micromachined impedance spectroscopy flow cytometer for cell analysis and particle sizing. Lab Chip 1(1):76–82
CrossRef

Gawad S, Cheung K, Seger U, Bertsch A, Renaud P (2004) Dielectric spectroscopy in a micromachined flow cytometer: theoretical and practical considerations. Lab Chip 4(3):241–251
CrossRef

Holmes D, She JK, Roach PL, Morgan H (2007) Bead-based immunoassays using a micro-chip flow cytometer. Lab Chip 7(8):1048–1056
CrossRef

Holmes D, Pettigrew D, Reccius CH, Gwyer JD, CV Berkel, Holloway J, Davies DE, Morgan H (2009) Leukocyte analysis and differentiation using high speed microfluidic single cell impedance cytometry. Lab Chip 9(20):2881–2889
CrossRef

Huh D, Gu W, Kamotani Y, Grotberg JB, Takayama S (2005) Microfluidics for flow cytometric analysis of cells and particles. Physiol Meas 26(3):R73–R98
CrossRef

Morgan H, Holmes D, Green NG (2006) High speed simultaneous single particle impedance and fluorescence analysis on a chip. Curr Appl Phys 6(3):367–370
CrossRef

Nieuwenhuis JH, Kohl F, Bastemeijer J, Sarro PM, Vellekoop MJ (2004) Integrated coulter counter based on 2-dimensional liquid aperture control. Sens Actuators B Chem 102(1):44–50
CrossRef

Rodriguez-Trujillo R, Castillo-Fernandez O, Garrido M, Arundell M, Valencia A, Gomila G (2008) High-speed particle detection in a micro-coulter counter with two-dimensional adjustable aperture. Biosens Bioelectron 24(2):290–296
CrossRef

Shapiro HM (1995) Practical flow cytometry, vol 3. Wiley, New York

Sohn LL, Saleh OA, Facer GR, Beavis AJ, Allan RS, Notterman DA (2000) Capacitance cytometry: measuring biological cells one by one. Proc Natl Acad Sci USA 97(20):10687–10690
CrossRef

Sun T, Morgan H (2010) Single-cell microfluidic impedance cytometry: a review. Microfluid Nanofluidics 8(4):423–443. doi:10.1007/s10404-010-0580-9
CrossRef

Zhang H, Chon C, Pan X, Li D (2009) Methods for counting particles in microfluidic applications. Microfluid Nanofluidics 7(6):739–749
CrossRef MATH

Over 8.5 million scientific documents at your fingertips
© Springer, Part of Springer Science+Business Media